Article

Alkali and Alkaline-Earth Metal Amidoboranes: Structure, Crystal Chemistry, and Hydrogen Storage Properties

Hui Wu, Wei Zhou, and Taner Yildirim

J. Am. Chem. Soc., **2008**, 130 (44), 14834-14839 • DOI: 10.1021/ja806243f • Publication Date (Web): 11 October 2008

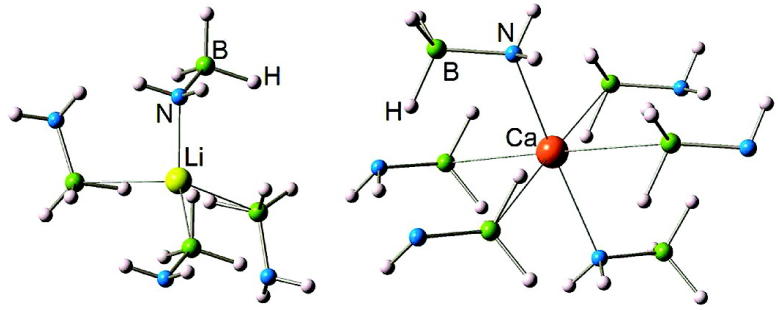

J|A|C|S
ARTICLES

Published on Web 10/11/2008

Alkali and Alkaline-Earth Metal Amidoboranes: Structure, Crystal Chemistry, and Hydrogen Storage Properties

Hui Wu,*[,†,‡] Wei Zhou,[†,‡] and Taner Yildirim[†,§]

NIST Center for Neutron Research, National Institute of Standards and Technology, Gaithersburg, Maryland 20899-6102, Department of Materials Science and Engineering, University of Maryland, College Park, Maryland 20742-2115, and Department of Materials Science and Engineering, University of Pennsylvania, Philadelphia, Pennsylvania 19104-6272

Received August 7, 2008; E-mail: huiwu@nist.gov

Abstract: Alkali- and alkaline-earth metal amidoboranes are a new class of compounds with rarely observed $[NH_2BH_3]^-$ units. $LiNH_2BH_3$ and solvent-containing $Ca(NH_2BH_3)_2 \cdot THF$ have been recently reported to significantly improve the dehydrogenation properties of ammonia borane. Therefore, metal amidoboranes, with accelerated desorption kinetics and suppressed toxic borazine, are of great interest for their potential applications for hydrogen storage. In this work, we successfully determined the structures of $LiNH_2BH_3$ and $Ca(NH_2BH_3)_2$ using a combined X-ray diffraction and first-principles molecular dynamics simulated annealing method. Through detailed structural analysis and first-principles electronic structure calculations the improved dehydrogenation properties are attributed to the different bonding nature and reactivity of the metal amidoboranes compared to NH_3BH_3.

Introduction

Ammonia borane (AB, NH_3BH_3), with 19.6 wt % hydrogen capacity, has recently attracted great interest due to its potential applications for chemical hydrogen storage. The NH_3BH_3 molecule contains both hydridic B−H and protic N−H bonds and a strong B−N bond so that hydrogen release from solid AB is more favorable than dissociation to ammonia and diborane under most conditions.[1] Solid AB releases 1 equiv of H_2 at temperatures up to 110 °C and forms a mixture of products consisting mostly of aminoborane oligomers, $[NH_2BH_2]_n$.[2−6] $[NH_2BH_2]_n$ can further dehydrogenate 1 equiv of H_2 at 110−200 °C and produce polyiminoboranes, $[NHBH]_n$.[2−4,7] However, accompanying the release of hydrogen, volatile toxic species such as borazine also form with increasing temperature ramp,[2−4,7] thus degrading the purity of hydrogen that can be used for fuel cell systems.

Several approaches, including use of various transition metals[8,9] and base−metal catalysts,[10] acid catalysis,[11] particle size effects from nanoscaffolds,[12] ionic liquids,[13] and carbon cryogels,[14] etc., have been reported to improve the dehydrogenation properties of AB in terms of the reduced dehydrogenation temperatures,[12] accelerated H_2 release kinetics,[8−14] and/or minimized borazine release.[13] However, there is no single approach that can achieve all these improvements simultaneously for AB. More recently, alkali metal amidoboranes, i.e., $LiNH_2BH_3$ and $NaNH_2BH_3$,[15] and solvent-containing alkaline-earth amidoborane, i.e., $Ca(NH_2BH_3)_2 \cdot 2THF$, [16] have been reported to show significantly enhanced dehydrogenation kinetics and suppressed borazine release.

Structural reports on compounds containing $[NH_2BH_3]^-$ are scarce. Although formation of $LiNH_2BH_3$, $NaNH_2BH_3$, and $Ca(NH_2BH_3)_2 \cdot 2THF$ has been identified in both solution[17,18] and the solid state[15,16] by NMR and X-ray diffraction (XRD),[15,16,18] to the best of our knowledge, no detailed crystal

[†] National Institute of Standards and Technology.
[‡] University of Maryland.
[§] University of Pennsylvania.

(1) Stephens, F.; Pons, V.; Baker, R. T. *Dalton Trans.* **2007**, 2613–2626.
(2) Hu, M. G.; Geanangel, R. A.; Wendlandt, W. W. *Thermochim. Acta* **1978**, *23*, 249–255.
(3) Baitalow, F.; Baumann, J.; Wolf, G.; Jaenicke-Rossler, K.; Leitner, G. *Thermochim. Acta* **2002**, *391*, 159–168.
(4) Wolf, G.; Baumann, J.; Baitalow, F.; Hoffmann, F. P. *Thermochim. Acta* **2000**, *343*, 19–25.
(5) Sit, V.; Geanangel, R. A.; Wendlandt, W. W. *Thermochim. Acta* **1987**, *113*, 379–382.
(6) Stowe, A. C.; Shaw, W. J.; Linehan, J. C.; Schmid, B.; Autrey, T. *Phys. Chem. Chem. Phys.* **2007**, *9*, 1831–1836.
(7) Baumann, J.; Baitalow, F.; Wolf, G. *Thermochim. Acta* **2005**, *430*, 9–14.
(8) Jaska, C. A.; Temple, K.; Lough, A. J.; Manners, I. *J. Am. Chem. Soc.* **2003**, *125*, 9424–9434.
(9) Denney, M. C.; Pons, V.; Hebden, T. J.; Heinekey, M.; Goldberg, K. I. *J. Am. Chem. Soc.* **2006**, *128*, 12048–12049.
(10) Keaton, R. J.; Blacquiere, J. M.; Baker, R. T. *J. Am. Chem. Soc.* **2007**, *129*, 1844–1845.
(11) Stephens, F. H.; Baker, R. T.; Matus, M. H.; Grant, D. J.; Dixon, D. A. *Angew. Chem., Int. Ed.* **2007**, *46*, 746–749.
(12) Gutowska, A.; Li, L.; Shin, Y.; Wang, C. M.; Li, X. S.; Linehan, J. C.; Smith, R. S.; Kay, B. D.; Schmid, B.; Shaw, W.; Gutowski, M.; Autrey, T. *Angew. Chem., Int. Ed* **2005**, *44*, 3578–3582.
(13) Bluhm, M. E.; Bradley, M. G.; Butterick, R.; Kusari, U.; Sneddon, L. G. *J. Am. Chem. Soc.* **2006**, *128*, 7748–7749.
(14) Feaver, A.; Sepehri, S.; Shamberger, P.; Stowe, A.; Autrey, T.; Cao, G. *J. Phys. Chem. B* **2007**, *111*, 7469–7472.
(15) Xiong, Z.; Yong, C. K.; Wu, G.; Chen, P.; Shaw, W.; Karkamkar, A.; Autrey, T.; Jones, M. O.; Johnson, S. R.; Edwards, P. P.; David, W. I. F. *Nat. Mater.* **2008**, *7*, 138–141.
(16) Diyabalanage, H. V. K.; Shrestha, R. P.; Semelsberger, T. A.; Scott, B. L.; Bowden, M. E.; Davis, B. L.; Burrell, A. K. *Angew. Chem., Int. Ed.* **2007**, *46*, 8995–8997.
(17) Schlesinger, H. I.; Burg, A. B. *J. Am. Chem. Soc.* **1938**, *60*, 290–299.
(18) Myers, A. G.; Yang, B. H.; Kopecky, D. J. *Tetrahedron Lett.* **1996**, *37*, 3623–3626.

 10.1021/ja806243f CCC: $40.75

structure information, i.e., atomic positions, has yet been published. The difficulty lies in several factors: the insensitivity of X-ray to light elements (e.g., H and Li), possible orientational disorder of $-NH_3$ and $-BH_3$ groups at room temperature, and various intermediate phases present in the samples. The reported structure of $Ca(NH_2BH_3)_2 \cdot 2THF$ includes organic solvent molecules, so that the Ca^{2+} cation in the structure bonds not only with $NH_2BH_3^-$ but also with oxygen ions.[16] This differs from the coordination environment of Ca^{2+} in the structure of solvent-free $Ca(NH_2BH_3)_2$ and thus results in the abnormal Ca−B and Ca−N bond distances, even shorter than those in $Ca(NH_2)_2$[19] and $Ca(BH_4)_2$.[20,21] In addition, the organic solvent contained releases accompanying the hydrogen, which not only complicates understanding of the dehydrogenation mechanism but degrades the purity of hydrogen desorbed. Removal of the solvent was reported to form amorphous $Ca(NH_2BH_3)_2$.[16] Therefore, the mechanisms of the improved dehydrogenation properties of $LiNH_2BH_3$ and $NaNH_2BH_3$ and solvent-free $Ca(NH_2BH_3)_2$ are not fully understood in part due to the lack of the crystal structure information.

In this study, we determined the crystal structures of representative alkali- and alkaline-earth amidoboranes, $LiNH_2BH_3$ (note that $NaNH_2BH_3$ is isostructural to $LiNH_2BH_3$[15]) and $Ca(NH_2BH_3)_2$, using combined X-ray diffraction and first-principles molecular dynamics simulations. The electronic structure and bonding characteristics of $LiNH_2BH_3$ and $Ca(NH_2BH_3)_2$ were investigated by first-principles calculations based on density function theory (DFT). With combined crystal and electronic structure information we further understood their improved dehydrogenation performance. Our study holds the key to understand the formation and stability of this new class of compounds and is critical for a rational improvement of hydrogen-storage properties of metal−amidoboranes and other possible amidoboranes with different substituents.

Experimental Section

Lithium amidoborane $LiNH_2BH_3$ and calcium amidoborane $Ca(NH_2BH_3)_2$ were prepared by ball milling stoichiometric ratios of LiH (95%, Aldrich)[22] and NH_3BH_3 (90%, Aldrich) (1:1), and CaH_2 (99%, Aldrich) and BH_3NH_3 (1:2) powders under 1 bar He. The $LiH-NH_3BH_3$ and $CaH_2-2NH_3BH_3$ mixtures were milled using a Fritsch Pulverisette 7 planetary mill at 200 rpm for 1 h and 350 rpm for various time (see Supporting Information), respectively. After milling, the mixtures were stored in a He-filled glovebox for further structural and property characterization. Graphite powders as a ball milling additive, as suggested in the previous study,[15] were also tested. The resulting structures and dehydrogenation properties of the products were found to be the same with or without the graphite additive. All sample handling was performed in the He-filled glovebox due to the extreme air sensitivity of these hydrides.

Phase identification and equilibrium were monitored on samples sealed in glass capillaries using a Rigaku X-ray diffractometer with a Cu K_α source. For the $LiH-NH_3BH_3$ mixture, a milling rate of more than 200 rpm or milling time longer than 60 min will cause partial decomposition of the $LiNH_2BH_3$ formed and formation of other phases. For $CaH_2-2NH_3BH_3$ mixture, extended and intense milling is needed to increase the yield of $Ca(NH_2BH_3)_2$. Data for structural study were collected over 24 h at room temperature in the 2θ range of 5−70° with a step size of 0.02°. The structures of these alkali or alkaline-earth amidoboranes were first partially solved using direct methods, which generated several candidate models with various $[NH_2BH_3]^-$ orientations due to the uncertain H positions from XRD data. First-principles molecular dynamics simulated annealing was then performed to help in determining the $[NH_2BH_3]^-$ configuration with the lowest energy among these models. Finally, Rietveld structural refinements on the optimal structural candidates were done using the GSAS package. The NH_2BH_3 complex was kept as a rigid body with common refined bond angles, and thermal parameters were fixed as reasonable values due to the inadequate number of observations. After refinement of the positions and orientations of the rigid body, the translation vectors of the rigid body, i.e., the bond lengths of B−N, B−H, and N−H, were also refined with certain restraints (see Tables S1 and S2, Supporting Information). One lithium atom and one NH_2BH_3 group for $LiNH_2BH_3$ and one calcium atom and one NH_2BH_3 group were refined for $Ca(NH_2BH_3)_2$ together with their corresponding lattice parameters in the final cycle, yielding the agreement factors of $R_{wp} = 0.0965$ and $R_p = 0.060$ for XRD data on $LiNH_2BH_3$ and $R_{wp} = 0.049$ and $R_p = 0.037$ for data on $Ca(NH_2BH_3)_2$, respectively. The slightly large R factors of the refined XRD pattern for $LiNH_2BH_3$ are due to the extra peaks from $Li(NH_2BH_3)(NH_3BH_3)$ phase and the impurity phases from unreacted LiH and NH_3BH_3 precursor (see Figures S1, S3, and S6, Supporting Information). The refined XRD patterns of $LiNH_2BH_3$ and $Ca(NH_2BH_3)_2$ are shown in Figures S1 and S2 in the Supporting Information. The atomic positions and bond lengths from refinements and calculations are listed in Tables S1 and S2 in the Supporting Information and Table 1.

Table 1. Experimental and calculated Bond Lengths[a]

		length (Å)	
	bond	exp	calcd
NH_3BH_3	N−B	1.58[27]	1.592
	N−H	1.07[27]	1.028/1.033
	B−H	1.18[27]	1.228/1.221
$LiNH_2BH_3$	Li−N	2.032	2.063
	N−B	1.561(7)	1.547
	N−H	1.025	1.025/1.026
	B−H	1.249	1.236/1.244/1.248
$Ca(NH_2BH_3)_2$	Ca−N	2.383	2.466
	N−B	1.575(4)	1.546
	N−H	1.027 /1.033	1.025/1.025
	B−H	1.263 /1.248/1.226	1.250/1.243/1.230

[a] Note that the B−H and N−H distances were restrained with standard deviation < 0.005 Å during refinement.

Dehydrogenation of $LiNH_2BH_3$ and $Ca(NH_2BH_3)_2$ was characterized by temperature-programmed desorption (TPD) performed on a Sieverts-type apparatus.[23]

The hydrogen-to-metal ratios in the hydride samples were checked using the neutron prompt-γ activation analysis (PGAA) facility, which is able to detect hydrogen as low as 2 μg.[24] Pure LiH and CaH_2 samples were used as standards to normalize γ-ray intensities. Disk sample configuration was used for all samples to decrease the amount of the neutrons absorbed by boron, and a long collecting time (~24 h) for each sample was adopted to obtain good statistics. The hydrogen-to-metal ratio in the ball-milled 1:1 ratio LiH/NH_3BH_3 is H:Li ≈ 5.32:1 ("$LiBNH_{5.32}$"), 1:2 ratio $LiH/2NH_3BH_3$ is H:Li ≈ 10.86:1 ("$LiB_2N_2H_{10.86}$"), and 1:2 $CaH_2/2NH_3BH_3$ is ≈ 11.08:1 ("$CaB_2N_2H_{11.08}$"). The stoichiometry of H was found to be approximately H:Li ≈ 1:1.32 ("$LiBNH_{1.32}$") and

(19) Senker, J.; Muller, M.; Press, W.; Muller, P.; Mayer, H. M.; Ibberson, R. M. *J. Phys. Chem. B* **1998**, *102*, 931–940.
(20) Buchter, F. *J. Phys. Chem. B* **2008**, *112* (27), 8042–8048.
(21) Miwa, K.; Aoki, M.; Noritake, T.; Ohba, N.; Nakamori, Y.; Towata, S.; Zuttel, A.; Orimo, S. *Phys. Rev. B* **2006**, *74*, 155122.
(22) Certain commercial suppliers are identified in this paper to foster understanding. Such identification does not imply recommendation or endorsement by the NIST nor does it imply that the materials or equipment identified are necessarily the best available for the purpose.
(23) Zhou, W.; Wu, H.; Hartman, M. R.; Yildirim, T. *J. Phys. Chem. C* **2007**, *111*, 16131.
(24) Lindstrom, R. M. *J. Res. Natl. Inst. Stand. Technol.* **1993**, *98*, 127–133.

H:Ca ≈ 1:2.233 ("$CaB_2N_2H_{2.33}$") in the dehydrogenated lithium amidoborane and calcium amidoborane.

Theoretical Calculations. First-principles calculations were performed within the plane-wave implementation of density functional theory (DFT) in the PWscf package.[25] We used a Vanderbilt-type ultrasoft potential with Perdew−Burke−Ernzerhof exchange correlation. A cutoff energy of 408 eV was found to be enough for the total energy and force to converge within 0.5 meV/atom and 0.005 eV/Å. Car−Parrinello molecular dynamics simulation[26] was used to help searching for the most likely crystal structures. The conventional unit cell was used with cell dimensions fixed at the experimental values. The initial system temperature was set to 600 K. The system was first allowed to evolve and equilibrate for 20 ps, and then the system temperature was slowly brought to 0 K in a period of 20 ps. Structure optimizations on the resulting candidate structures at 0 K were further performed with respect to atomic positions with the lattice parameters fixed at the experimental values. Lattice dynamics calculations were then performed on the relaxed structures to rule out unstable candidates. The total energies of the stable candidate structures at 0 K, including corrections for the zero-point motion, were also evaluated. This information was used in combination with XRD pattern matching to derive the best crystal structure solutions of the metal amidoboranes.

Results and Discussions

Crystal Structure and Electronic Structure of $LiNH_2BH_3$ and $Ca(NH_2BH_3)_2$. Most of the reflections in the XRD pattern collected on the ball-milled 1:1 ratio of LiH and NH_3BH_3 mixture can be indexed using a *Pbca* (No. 61, $Z = 8$) cell with $a = 7.1051(8)$ Å, $b = 13.930(1)$ Å, and $c = 5.1477(7)$ Å, consistent with the previous report.[15] Besides these peaks, we observed extra peaks which were also present in the previously reported patterns but not indexed,[15] e.g., peaks at $d \approx 8.54$, 3.93 Å, etc. (Figure S1, Supporting Information). These peaks are not from the unreacted LiH and NH_3BH_3 precursors. When the LiH to NH_3BH_3 ratio decreases, these peaks became more prominent and the peak intensities from the *Pbca* cell weaken (see Figure S3, Supporting Information). At a 1:2 ratio of LiH and NH_3BH_3, reflections from the *Pbca* cell disappear and only these extra peaks remain. These remaining peaks can be indexed using a $Cmc2_1$ orthorhombic cell (Figure S4, Supporting Information). For the ball-milled mixture of $CaH_2/2NH_3BH_3$, all peaks other than the unreacted precursors can be indexed using a monoclinic *C*2 (No. 5, $Z = 2$) cell with $a = 9.100(2)$ Å, $b = 4.371(1)$ Å, $c = 6.441(2)$ Å, and $\beta = 93.19°$, which is different from the reported $Ca(NH_2BH_3)(THF)_2$ solvent-containing compound.[16] With the indexed lattice parameters, the crystal structures of 1:1 lithium amidoborane and 1:2 calcium amidoborane were then solved using combined direct methods and first-principles molecular dynamics simulated annealing, which revealed a stoichiometry of $LiNH_2BH_3$ and $Ca(NH_2BH_3)_2$, respectively, consistent with elemental analysis from PGAA measurements. It can be seen from inspection of the XRD data that all the reflections of $LiNH_2BH_3$ and $Ca(NH_2BH_3)_2$ can be fitted very well using the determined structure models (Figures S1 and S2, Supporting Information), which strongly supports the validity of our structure solutions. More accurate structural details, such as individual B−H and N−H bond lengths and bond angles, can be easily obtained by refining neutron diffraction data on the isotope-enriched samples in the future. For the 1:2 LiH: NH_3BH_3 phase, the structure at room temperature was solved using the $Cmc2_1$ cell, which reveals a stoichiometry of $Li(NH_2BH_3)(NH_3BH_3)$, also in agreement with the PGAA results. In this structure the $NH_2BH_3^-$ ions have definite orientation to bond with Li^+ ions while NH_3BH_3 units tend to orientational disorder at room temperature, similar to the known disordered structure of NH_3BH_3 at room temperature.[27] The calculated XRD pattern based on the structure determined by direct methods shows good agreement overall with the observed patterns (see Figure S4, Supporting Information). Due to its intermediate nature, DFT electronic structure calculations were not performed on this phase. We focus on the determined structures of $LiNH_2BH_3$ and $Ca(NH_2BH_3)_2$, which allows us to do further theoretical calculations on their electronic structures and energetics to better understand the formation and nature of this new class of alkali and alkaline-earth amidoborane compounds.

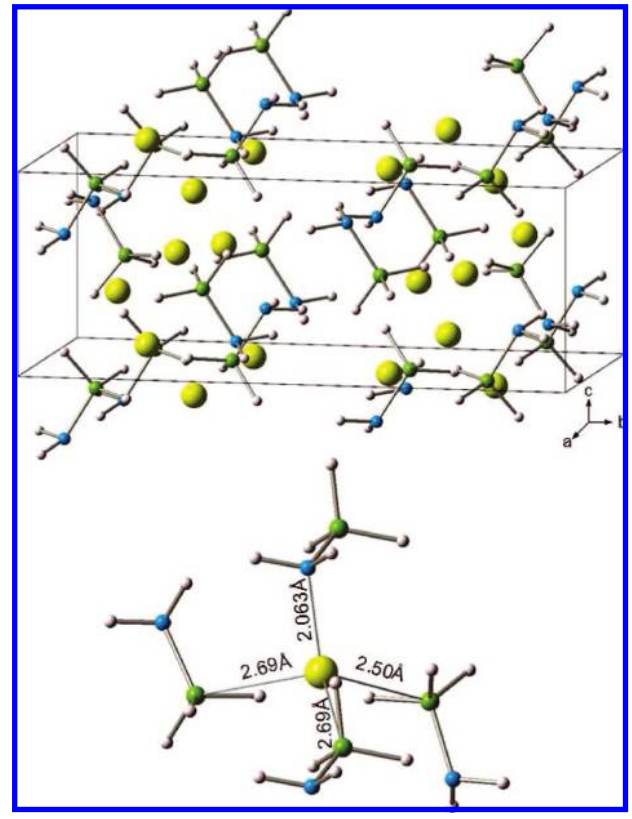

Figure 1. (Top) Crystal structure of $LiNH_2BH_3$ as determined in this study. Li, B, N, and H atoms are represented by yellow, green, blue, and white spheres, respectively. (Bottom) Coordination environment of Li^+. Each Li^+ is coordinated with four $NH_2BH_3^-$ ions with one Li−N bond length of 2.06 Å and three Li−B distances of 2.50−2.69 Å.

Figures 1 and 2 show the derived crystal structures for $LiNH_2BH_3$ and $Ca(NH_2BH_3)_2$. In $LiNH_2BH_3$, the distance between Li^+ and N in the nearest $[NH_2BH_3]^-$ ion is 2.063 Å, similar to the Li−N distances (2.06−2.21Å) in the ionic compound $LiNH_2$.[28] In addition, each Li^+ is also surrounded by three other $[NH_2BH_3]^-$ ions with Li−B distances in the range

(25) Baroni, S.; Dal Corso, A.; de Gironcoli, S.; Giannozzi, P.; Cavazzoni, C.; Ballabio, G.; Scandolo, S.; Chiarotti, G.; Focher, P.; Pasquarello, A.; Laasonen, K.; Trave, A.; Car, R.; Marzari, N.; Kokalj, A. Quantum-ESPRESSO; http://www.pwscf.org/.
(26) Car, R.; Parrinello, M. *Phys. Rev. Lett.* **1985**, *55*, 2471.
(27) (a) Hughes, E. W. *J. Am. Chem. Soc.* **1956**, *78*, 502. (b) Hoon, C. F.; Reynhardt, E. C. *J. Phys. C.* **1983**, *16*, 6129. (c) Buehl, M.; Steinke, T.; von Ragué Schleyer, P.; Boese, R. *Angew. Chem., Int. Ed.* **1991**, *30*, 1160. (d) Klooster, W. T.; Koetzle, T. F.; Siegbahn, P. E. M.; Richardson, T. B.; Crabtree, R. H. *J. Am. Chem. Soc.* **1999**, *121*, 6337.
(28) Nagib, M.; Jacob, H. *Z. Anorg. Allg. Chem.* **1972**, *391*, 271.

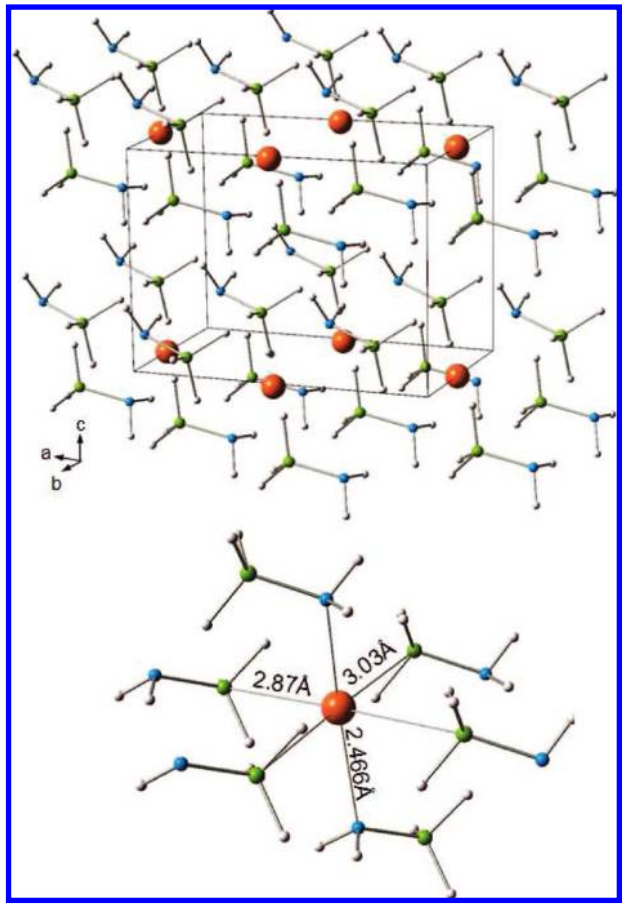

Figure 2. (Top) Crystal structure of $Ca(NH_2BH_3)_2$ as determined in this study. Ca, B, N, and H atoms are represented by orange, green, blue, and white spheres, respectively. (Bottom) Coordination environment of Ca^{2+}. Each Ca^{2+} is coordinated with six $NH_2BH_3^-$ ions with two Li−N bond lengths of 2.46 Å and four Li−B distances of 2.87 and 3.03 Å.

of 2.50−2.69 Å, close to the Li−B distances (2.37−2.62 Å) in $LiBH_4$.[29] Therefore, each Li^+ is actually coordinated with four $[NH_2BH_3]^-$ groups, consistent with the Li (IV) tetrahedral coordination preferred in the commonly observed complex hydrides, e.g., $LiNH_2$,[28] $LiBH_4$,[29] Li_2BNH_6, and $Li_4BN_3H_{10}$.[30] In $Ca(NH_2BH_4)_2$, each Ca^{2+} directly bonds with two $[NH_2BH_3]^-$ ions with the closest Ca−N distance of ∼2.466 Å, similar to those in $Ca(NH_2)_2$ (Ca−N = 2.441−2.573Å).[19] Each Ca^{2+} is also coordinated with the other four $[NH_2BH_3]^-$ groups with a Ca−B distance in the range of 2.87−3.03 Å, aligning with those distances (2.89−2.96 Å) in $Ca(BH_4)_2$.[20,21] Therefore, Ca^{2+} in $Ca(NH_2BH_3)_2$ also satisfies its octahedral coordination preference (VI) in the Ca-related complex hydrides, e.g., $Ca(NH_2)_2$,[19] CaNH,[31] and $Ca(BH_4)_2$.[20,21]

The B−N bond lengths in $LiNH_2BH_3$ and $Ca(NH_2BH_3)_2$ are 1.547 and 1.546 Å, respectively, both shorter than that (∼1.58 Å) in solid NH_3BH_3,[27,32] which indicates a stronger bonding between B and N in the alkali and alkaline-earth metal−amidoborane compounds. In addition, in these structures the B−N−Li and B−N−Ca bond angles are 113° and 116°, respectively, similar to the H−N−B bond angles (109−114°).

Table 2. Mulliken Population Analysis of Charge Densities

	NH_3BH_3	$LiNH_2BH_3$	$Ca(NH_2BH_3)_2$
Li/Ca		+0.98	+1.67
N	−0.89	−0.94	−1.00
H(on N)	+0.45/+0.44	+0.34	+0.38/+0.38
B	−0.30	−0.33	−0.28
H(on B)	−0.06/−0.04	−0.17/−0.12/−0.10	−0.13/−0.10/−0.09

Note that the Li−N and Ca−N bonds are not bent toward the B−N bond, as suggested by previous theoretical calculations on the isolated molecular $LiNH_2BH_3$ and $Ca(NH_2BH_3)_2$ complexes.[33]

The DFT-calculated B−H and N−H bond lengths after structural optimization are ∼1.244 and 1.025 Å in $LiNH_2BH_3$ and ∼1.241 and 1.025 Å in $Ca(NH_2BH_3)_2$, respectively. Refined B−H and N−H bond lengths from the rigid body are 1.249 and 1.025 Å for $LiNH_2BH_3$ and ∼1.245 and ∼1.03 Å in $Ca(NH_2BH_3)_2$. Although the refined bond lengths from the XRD data are not accurate, they are consistent with the calculations. The N−H bonds in $LiNH_2BH_3$ and $Ca(NH_2BH_3)_2$ are similar to the N−H bonds in solid NH_3BH_3 crystal structure, while the B−H bond lengths are longer than those in solid NH_3BH_3, indicating the similar N−H covalent bonds but the weakened covalent characteristics of B−H bonds. The calculated shortest BH···HN intermolecular distance (H−H distance) is 2.249 Å in $LiNH_2BH_3$ and 2.328Å in $Ca(NH_2BH_3)_2$, which is longer than those in solid NH_3BH_3 (2.02 Å)[27d] but still slightly less than 2.4 Å, the van der Waals distance for the interaction constituting a dihydrogen bond.[1]

To further understand the bonding nature in this new class of compounds, we analyzed their electronic structures. The calculated Mulliken charges[34] are listed in Table 2. Consistent with the above structural determination on the bond lengths, our calculations show a significant ionic character between and $NH_2BH_3^-$ and Li/Ca cations with a Mulliken charge of +0.98 on Li and +1.67 on Ca, close to their formula valences. The hydrogen on nitrogen becomes less charged in $LiNH_2BH_3$ and $Ca(NH_2BH_3)_2$ than in NH_3BH_3 because N attracts more electrons directly from the metal. In contrast, the hydrogen on boron in $LiNH_2BH_3$ and $Ca(NH_2BH_3)_2$ shows increased ionic character, i.e., more negative charged H on B, than that in NH_3BH_3. This suggests that H on B in $LiNH_2BH_3$ and $Ca(NH_2BH_3)_2$ will be a stronger Lewis base and more reactive than the H−B bond in NH_3BH_3. In Figure S8 (Supporting Information) we show the total electron densities of states (DOS) and their projections around the different atomic sites for the three compounds. Some common features are obvious. Particularly, the states of H bonded to N are in regions of lower energy while hydrogen bonded with boron accounts for most of the states in the region close to the Fermi level, indicating the H−B bond is more reactive than the H−N bond in general. Previous calculations in polyiminoborane and polyborazylene also suggested that H−B is a more ionic bond than H−N.[32] The DOS of $LiNH_2BH_3$ and $Ca(NH_2BH_3)_2$ also exhibits some distinctive features compared to that of solid NH_3BH_3. For example, a large number of the states of N in $LiNH_2BH_3$ and $Ca(NH_2BH_3)_2$ are promoted to the region closer to the Fermi level, in agreement with the more charged N and stronger N−B hybridization in $LiNH_2BH_3$

(29) Hartman, M. R.; Rush, J. J.; Udovic, T. J.; Bowman, R. C., Jr.; Hwang, S. J. *J. Solid State Chem.* **2007**, *180*, 1298.
(30) Wu, H.; Zhou, W.; Udovic, T. J.; Rush, J. J.; Yildirim, T. *Chem. Mater.* **2008**, *20*, 1245.
(31) Sichla, T.; Jacobs, H. *Z. Anorg. Allg. Chem.* **1996**, *622*, 2079–2082.
(32) Miranda, C. R.; Ceder, G. *J. Chem. Phys.* **2007**, *126*, 184703.
(33) Armstrong, D. R.; Perkins, P. G.; Walker, G. T. *J. Mol. Struct. (THEOCHEM)* **1985**, *23*, 189–203.
(34) Szabo, A.; Ostlund, N. S. *Modern Quantum Chemistry*; McGraw-Hill: New York, 1989.

and $Ca(NH_2BH_3)_2$ than in NH_3BH_3 (Table 2). Overall, with accepting electrons from strong alkali or alkaline-earth metals, the charge density distribution and bonding natures of solid NH_3BH_3 are dramatically altered in these new compounds.

Formation and Dehydrogenation of $LiNH_2BH_3$ and $Ca(NH_2BH_3)_2$. As in the previous work,[15] the $LiNH_2BH_3$ and $Ca(NH_2BH_3)_2$ compounds in the present study were formed by ball milling NH_3BH_3 and the corresponding metal hydrides instead of using pure Li or Ca metal. Therefore, formation of these compounds cannot be simply rationalized by substitution of H with the more electron-donating elements as proposed previously.[15] To understand formation of these metal amidoborane compounds, it is useful to make reference to the general Lewis base and acid reactions. The hydride anion H^- is known as a strong Lewis base, i.e., an active electron-donating species. When hydride is mixed with NH_3BH_3, H^- in the hydride attacks the protic hydrogen atom on nitrogen of NH_3BH_3, in other words, Lewis base H^- and $NH_2BH_3^-$ compete with each other to combine with the proton Lewis acid, H^+. H^- in LiH and CaH_2 is a stronger base than $NH_2BH_3^-$. Therefore, the protic hydrogen atom transfers from NH_3BH_3 to H^-, generating H_2 molecules. Li^+ or Ca^{2+} cations then subsequently combine with $NH_2BH_3^-$ ions and form ionic compounds $LiNH_2BH_3$ or $Ca(NH_2BH_3)_2$. For a stronger Lewis base with a cation of stronger ionicity, e.g., NaH, it will be more facile for deprotonation to occur and generate the metal amidoborane compound, as observed in $NaNH_2BH_3$.[15] If hydrogen in these hydrides cannot obtain enough electrons from its metal cation donor, the hydride will be a relatively weaker Lewis base and not be capable of acquiring the protic hydrogen atom from NH_3BH_3 to form amidoborane. This is confirmed by the observation that no metal amidoborane compounds can be formed by milling $MgH_2/2NH_3BH_3$ and $TiH_2/2NH_3BH_3$ mixtures. MgH_2 (or TiH_2) and NH_3BH_3 remain after ball milling under various conditions (see Figures S9 and S10, Supporting Information). The milled MgH_2 or TiH_2 also do not participate in the dehydrogenation process of NH_3BH_3, as observed by Mg metal forming and TiH_2 remaining in the XRD patterns after dehydrogenation (Figures S9, S10, and S11, Supporting Information).

The TPD measurement was performed on $LiNH_2BH_3$ and $Ca(NH_2BH_3)_2$ to study their dehydrogenation properties. Dehydrogenation of milled pure NH_3BH_3 was also measured for comparison. Figure 3 shows the TPD results. Pure NH_3BH_3 releases ~1.8 equiv of H_2/mol of BH_3NH_3 at ~110 and ~155 °C. $LiNH_3BH_3$ releases most of the hydrogen at ~92 and 120 °C within 3 h. PGAA element analysis of the samples after TPD study up to 200 °C indicates a composition of $\sim LiBNH_{1.32}$. Unlike the solvent-containing $Ca(NH_2BH_3)_2 \cdot 2THF$, which releases organic molecules in addition to hydrogen, our solvent-free $Ca(NH_2BH_3)_2$ shows a cleaner desorption profile with explicit hydrogen desorption temperatures. $Ca(NH_2BH_3)_2$ starts to desorb hydrogen at ~80 °C with vigorous hydrogen release at ~100 and 140 °C. There is a small hydrogen desorption peak at 110 °C, which could be due to the unreacted NH_3BH_3 precursor. After the reaction finished at 250 °C, ~2 equiv of H_2 (per $1/2Ca(NH_2BH_3)_2$) were desorbed with a composition of $\sim CaB_2N_2H_{2.33}$ from the TPD samples. XRD on the products of these alkali and alkaline-earth metal amidoboranes after desorption indicated formation of amorphous phases, which prevents direct determination of their structures. After dehydrogenation, both $LiNH_2BH_3$ and $Ca(NH_2BH_3)_2$ could not be rehydrogenated within the currently studied temperature range under 50 bar H_2 pressure. Comparing the reported NMR data

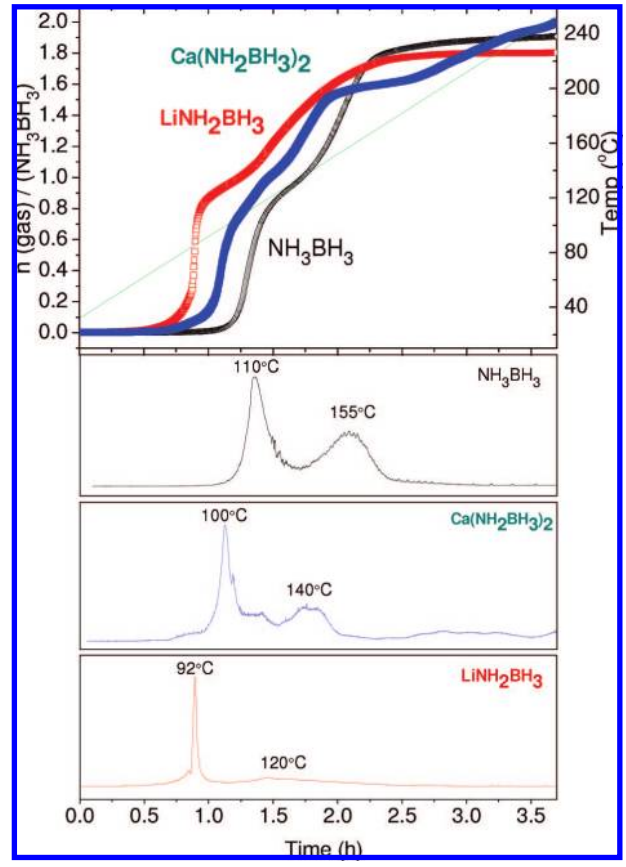

Figure 3. TPD results of hydrogen release for $LiNH_2BH_3$, $Ca(NH_2BH_3)_2$, and NH_3BH_3 with a 1 °C/min heating ramp. Dehydrogenation of $LiNH_2BH_3$ and $Ca(NH_2BH_3)_2$ begins at lower temperatures than NH_3BH_3. The amount of hydrogen gas released has been normalized as *n* (H_2 gas)/mol of NH_3BH_3.

on the dehydrogenated $LiNH_2BH_3$[15] with previous studies in the dehydrogenated NH_3BH_3,[13] the chemical shift of +29.8 ppm is consistent with the observed formation of internal B═N or terminal B═NH_2 units. Moreover, in agreement with the reported dehydrogenation studies,[15,16] we found that the notable features of dehydrogenation of these metal amidoboranes are the suppressed release of borazine during dehydrogenation and enhanced desorption kinetics at low temperatures.

The improved dehydrogenation properties of alkali metal amidoboranes have been ascribed to the presence of both positive and negative hydrogen and avoidance of mass transport through different phases as for the amide−hydride combination.[15] However, the protic and hydridic hydrogens are actually present in the pure NH_3BH_3 as well. The recently reported enhanced dehydrogenation of NH_3BH_3, with the aid of ionic liquids,[13] acids,[11] and catalysts,[8−10] also does not involve an interface reaction and mass transport through different phases. Instead, we propose that the changes in the reaction kinetics reflect the different reactivity of hydrogen in the alkali or alkaline-earth metal amidoboranes and pure solid NH_3BH_3. As noted previously, more reactive intermediates or transition states, such as the diammoniate of diborane $[(NH_3)_2BH_2]^+[BH_4]^-$[6] and/or BH_4^- formed by dehydrogenation of NH_3BH_3 in ionic liquids[13] and the borenium cation $[H_2B{-}NH_3]^+$ produced in acid initiation of NH_3BH_3 dehydrogenation,[11] have been shown to effectively enhance dehydrogenation and reduce the borazine release. Therefore, the decreased dehydrogenation temperatures of $LiNH_2BH_3$ and $Ca(NH_2BH_3)_2$ compared to solid AB are more

likely related to their crystal structures and the resulting changes in the nature and reactivity of hydrogens.

As described in the previous section, with more electrons being donated from metal to $[NH_2BH_3]^-$ ions, the hydridic B−H bond of $[NH_2BH_3]^-$ ions is increased, which enhances its activity compared to those in NH_3BH_3. This effect is similar to the active intermediate BH_4^- induced by the ionic liquid. Therefore, the barrier of the reaction between $[NH_2BH_3]^-$ ions would be lower than that between two neutral NH_3BH_3 molecules. In addition, the charged $[NH_2BH_3]^-$ ion creates more polar surroundings compared to the symmetric NH_3BH_3 complex. As proposed for the enhanced dehydrogenation of NH_3BH_3 in ionic liquids, the reaction environment controls the course of hydrogen release.[13] Compared to reactions between NH_3BH_3 in solid AB, the polar environments of the $[NH_2BH_3]^-$ ions coupled with a change in the reactivity among these ions in the metal amidoborane compounds will facilitate B−H···H−N interactions between the adjacent $[NH_2BH_3]^-$ ions. Even though we do not have enough information to determine the reaction pathway and the dehydrogenation products, it is tempting to conclude that the electronic and structural changes from NH_3BH_3 to $[NH_2BH_3]^-$ are the main reasons for the observed improved hydrogen release process/kinetics.

Identification of the dehydrogenation products is still necessary in the future, which will enable direct comparison of the reaction enthalpies and barriers between metal amidoboranes and NH_3BH_3 through first-principles reaction path calculations and thus promote further studies to achieve the possible reversibility of these materials.

Conclusions

We successfully prepared solvent-free alkali and alkaline-earth metal amidoboranes, i.e., lithium amidoborane $LiNH_2BH_3$ and calcium amidoborane $Ca(NH_2BH_3)_2$. Their crystal structures have been determined using combined X-ray diffraction and molecular dynamics simulated annealing methods. The desorption results showed that the alkali and alkaline-earth metal amidoboranes not only provide high hydrogen storage capacity but also exhibit dramatically improved dehydrogenation properties compared to pure solid ammonia borane (NH_3BH_3). From crystal structure analysis and a dehydrogenation study combined with the first-principles DFT calculations, the reduced dehydrogenation temperature is likely related to the different bonding nature and reactivity of the metal amidoboranes compared to NH_3BH_3. Similar to NH_3BH_3 in acid or ionic liquid, these results suggest that the dehydrogenation properties of NH_3BH_3 in the solid state may also be significantly improved by tuning the reactivity of B−H and/or N−H through inducing polar species such as strong electropositive cations or highly active anions (e.g., NH_2^- and BH_4^-).

Acknowledgment. This work was partially supported by the DOE through BES grant no. DE-FG02-08ER46522 (T.Y.).

Supporting Information Available: Crystal structure information of $LiNH_2BH_3$ and $Ca(NH_2BH_3)_2$, refined and calculated atomic positions and refined XRD patterns; calculated vibrational frequencies of $LiNH_2BH_3$ and $Ca(NH_2BH_3)_2$; structure variation of the $LiH-NH_3BH_3$ binary system with different LiH: NH_3BH_3 ratios; structure information of $LiNH_2BH_3(NH_3BH_3)$ (1:2 phase); calculated density of states (DOS) of $LiNH_2BH_3$, $Ca(NH_2BH_3)_2$, and NH_3BH_3; structural and dehydrogenation studies of other mixed metal hydride (i.e., MgH_2 and TiH_2) and NH_3BH_3 systems; proposed possible reaction pathways and dehydrogenation products; complete ref 20. This material is available free of charge via the Internet at http://pubs.acs.org.

JA806243F